# RESULTS OF POLOIDAL OHMIC HEATING IN A TOROIDAL OCTUPOLE

D.J. Holly
S.C. Prager
J.C. Sprott

PLP 818

November 1979

Plasma Studies

University of Wisconsin

## INTRODUCTION

As multipole plasmas are being pushed into higher energies, both for general plasma studies and for assessment as advanced fuel reactors, it is desirable to examine various methods of heating them. One such method is poloidal ohmic heating. Poloidal ohmic heating of an octupole may have advantages over the toroidal ohmic heating used in stellarators and tokamaks. The deep octupole magnetic mirrors provide enhanced resistivity; this may be an advantage over toroidal ohmic heating, allowing large power deposition into the plasma for a given current magnitude. Also, it is not known whether a current limit exists for this type of heating. This paper describes poloidal ohmic heating experiments carried out in Tokapole II since about a year ago. For these experiments Tokapole II is changed from its usual Tokamak-like operation to operation in the octupole mode, with the plasma current driven poloidally instead of toroidally.

The results of our poloidal ohmic heating experiments so far indicate an enhanced resistivity as expected; large values of ohmic power (>1 MW) are coupled into the plasma, but confinement is seriously degraded by the heating. The ion saturation current fluctuation level is greatly increased

by the ohmic heating, and the transport produced by these fluctuations appears consistent with the observed confinement time.

## FIELD TIMING

In order to drive current in the poloidal direction, the fields are set up as shown in Fig. 1. $H_2$ gas is puffed in through a fast puff valve; about 10 msec later the octupole field is brought up and crowbarred. A poloidal electric field is then created by discharging a separate capacitor bank into the toroidal field windings. (This also produces a toroidal magnetic field.) The poloidal electric field is created shortly after the octupole crowbar, so that the octupole field is roughly constant and the electric field is almost purely poloidal. The poloidal field bank is set up as for a standard Tokapole II shot; the $B_T$ bank is reduced to 24 240 uf capacitors and the $B_T$ windings are set at a 48:1 ratio instead of the usual 96:1. Microwave preionization is needed to initiate the discharge; there is little difference in the ohmic discharges initiated with 50 W S-band preionization (2.45 GHz), producing ECRH resonant zones near the center of the machine, and those initiated with 10 kW X-band (8.8 Ghz), producing ECRH resonant zones near the rings. Generally the X-band is used alone, or both the X- and S-band sources are

Figure 1. Field timing for poloidal ohmic heating in Tokapole II.

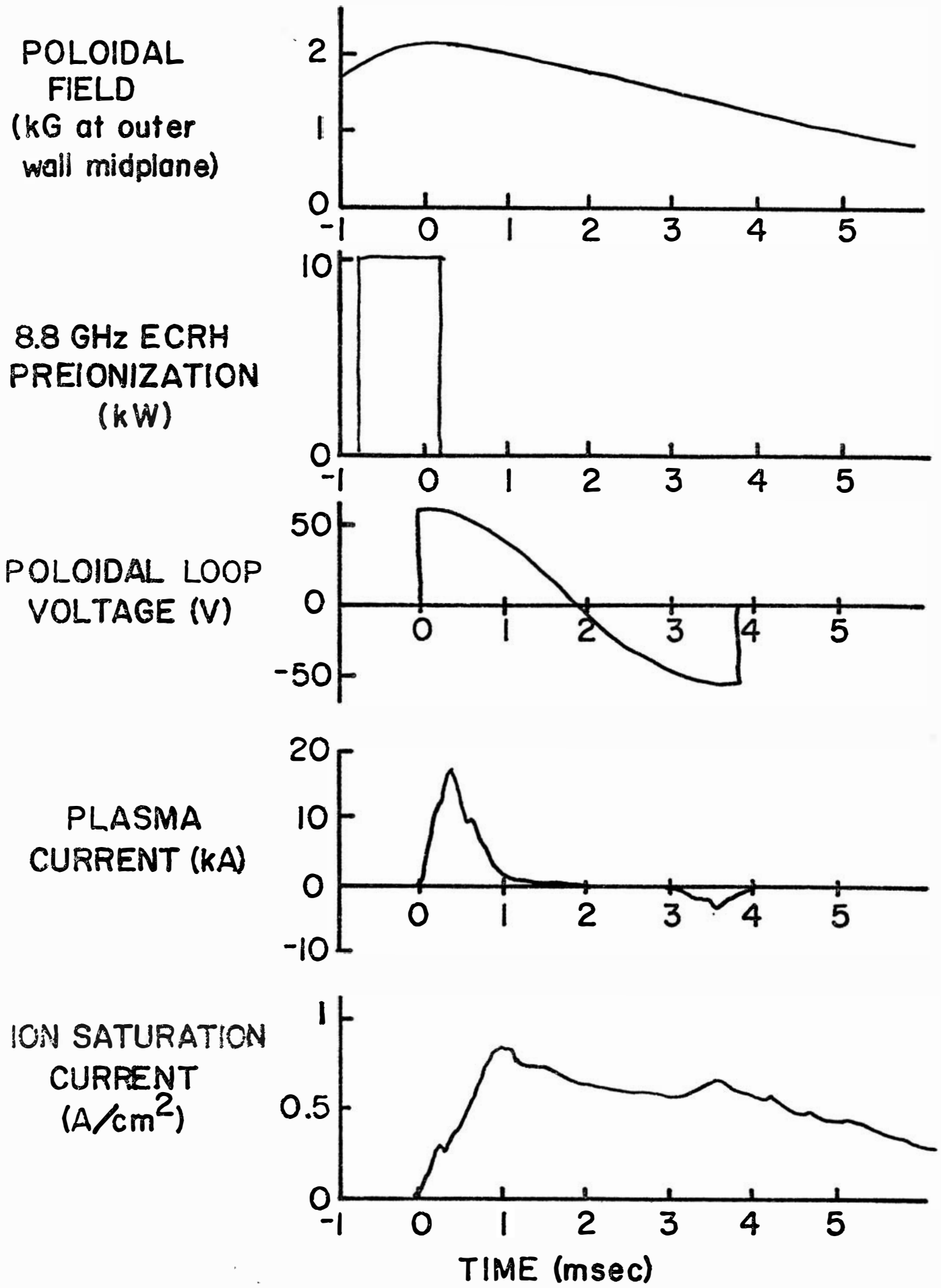

used. The plasma current peaks at about .5 msec and is always much smaller on the second (negative) half-cycle of the poloidal loop voltage than on the first half-cycle. Typical magnitudes are indicated in Fig. 1.

## POLOIDAL CURRENT MEASUREMENTS

The poloidal plasma current can be measured by measuring the change it produces in the toroidal magnetic field. The toroidal field is the sum of the field due to the windings and the field due to the poloidal plasma current:

$$B_T = \frac{\mu_0}{2\pi R}(I_W + I_P)$$

$$= \frac{\mu_0}{2\pi R}(I_{W(VAC)} + \Delta I_W + I_P)$$

$$= B_{T(VAC)} + \Delta B_T$$

where $I_W$ is the primary winding current, $I_P$ is the poloidal plasma current, the subscript VAC indicates quantities in the absence of plasma, and $\Delta$ indicates the change due to the poloidal plasma current.

Since the probe responds to the net current flowing between it and the inside wall, the plasma current density profile can be obtained by making a radial scan of the plasma current:

$$j(R) = \frac{1}{2\pi R} \frac{\partial}{\partial R} I_R$$

where $I_R$ is the net current between radius R and the major axis.

The probe consists of a 500-turn coil of fine copper wire about 1 cm long inside a 1/4-inch diameter tube of 15-mil stainless steel. The coil is wound on a G-10 form and is coated with two-component RTV, and can be quickly replaced by pulling it from the stainless steel tube and soldering a new coil in its place. The probe's frequency response is flat up to about 300 kHz. The probe is inserted through a port into the major axis on the midplane and oriented as in Fig. 2, so that the probe output is proportional to $\dot{B}_T$.

The circuit of Fig. 3 is used to extract the poloidal current from the $\dot{B}_T$ measurement. The plasma current signal is only a few percent of the winding signal upon which it is superimposed, so it is not trivial to accurately separate the plasma current signal. First the fields are fired without

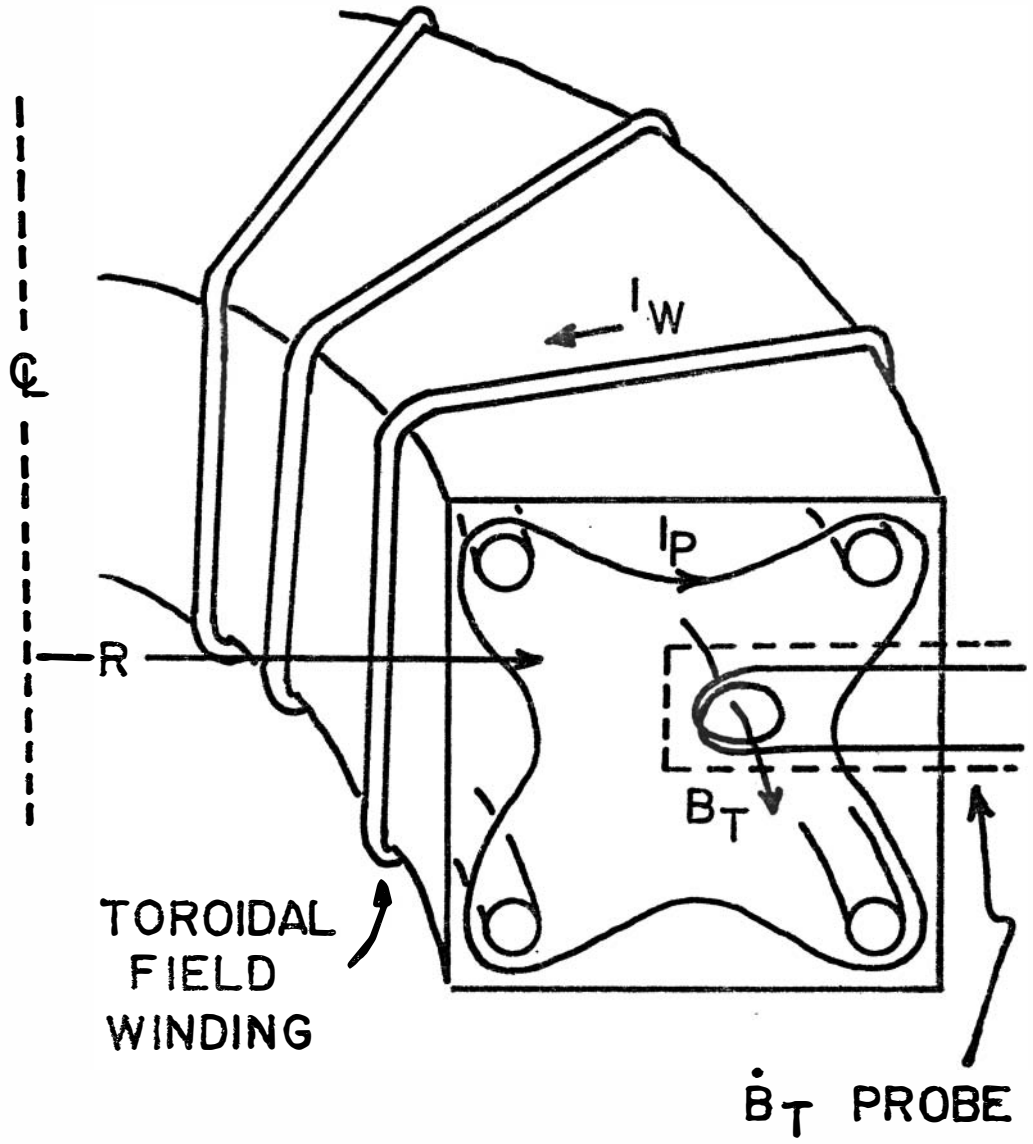


Figure 2. Measuring poloidal plasma current with a $\dot{B}_T$ probe.

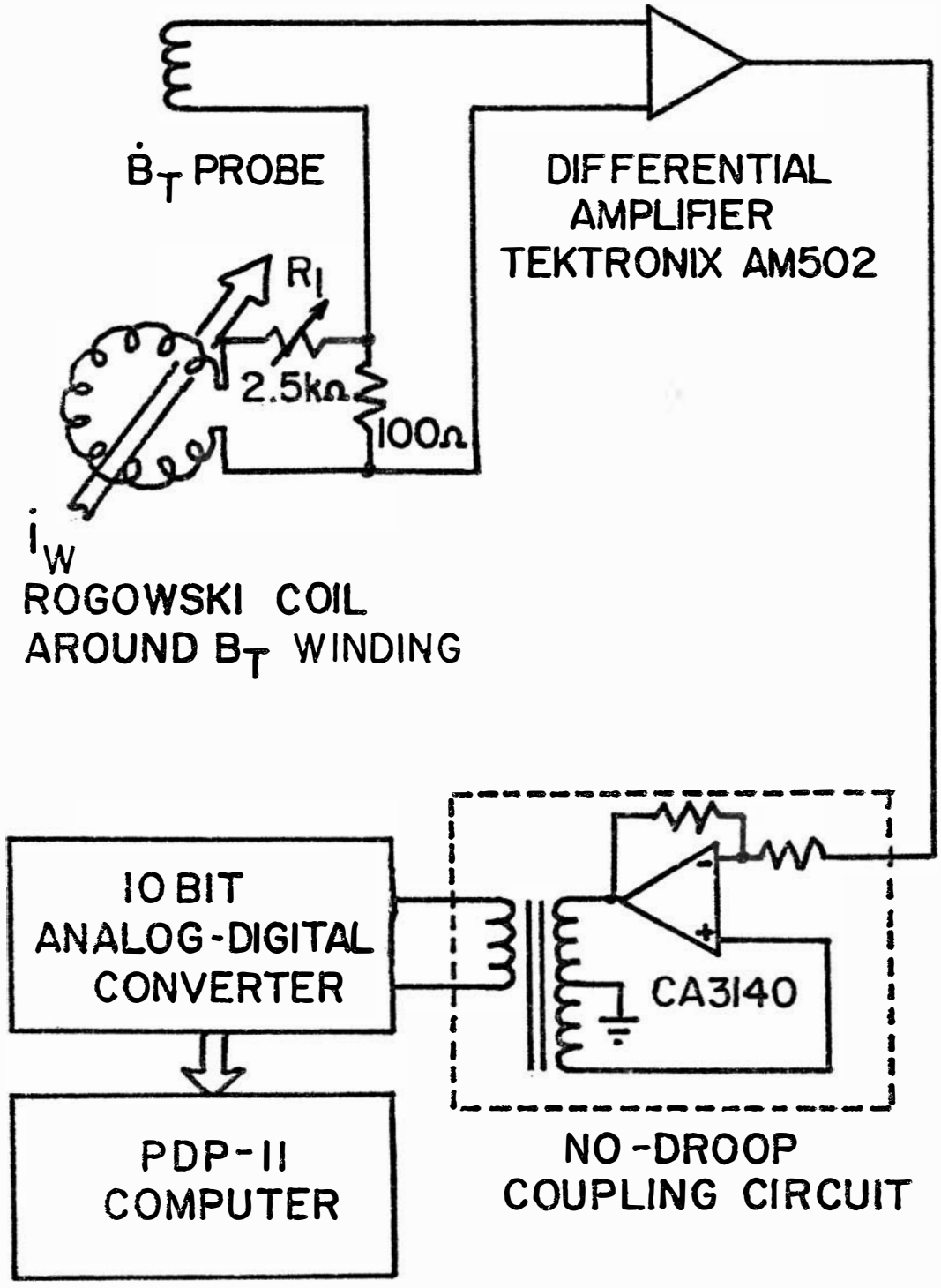


Figure 3. Circuit used to extract poloidal plasma current from $B_T$ measurement.

puffing any gas, so that no plasma is produced, and $R_1$ is adjusted until the winding current signal from the Rogowski coil cancels the $\dot{B}_T$ signal from the probe. Then the machine is pulsed with plasma and the nulled signal, after integration, is directly proportional to the poloidal plasma current:

$$I_P = \frac{2\pi R}{\mu_0} \Delta B_T - \Delta I_W$$

In practice the nulling is not perfect so the computer must take a no-plasma baseline for each shot and subtract it. This leads to an error of $\epsilon I_W$ in the measured plasma current, where $\epsilon$ is the ratio of the nulled signal to the un-nulled signal. Since $\epsilon$ is typically a few percent and since $\Delta I_W$ is on the order of $I_P$, imperfect nulling leads to errors of only a few percent in measuring the plasma current.

A typical $I_P$ waveform obtained this way is shown in Fig. 4. To prevent droop problems the coupling circuit[1] shown schematically in Fig. 3, rather than a simple transformer, is used to isolate the signal path to the computer. Also, the signal integration is done by the computer, to minimize noise pickup and droop. The circuit is calibrated by measuring the un-nulled vacuum $B_T$ signal; then

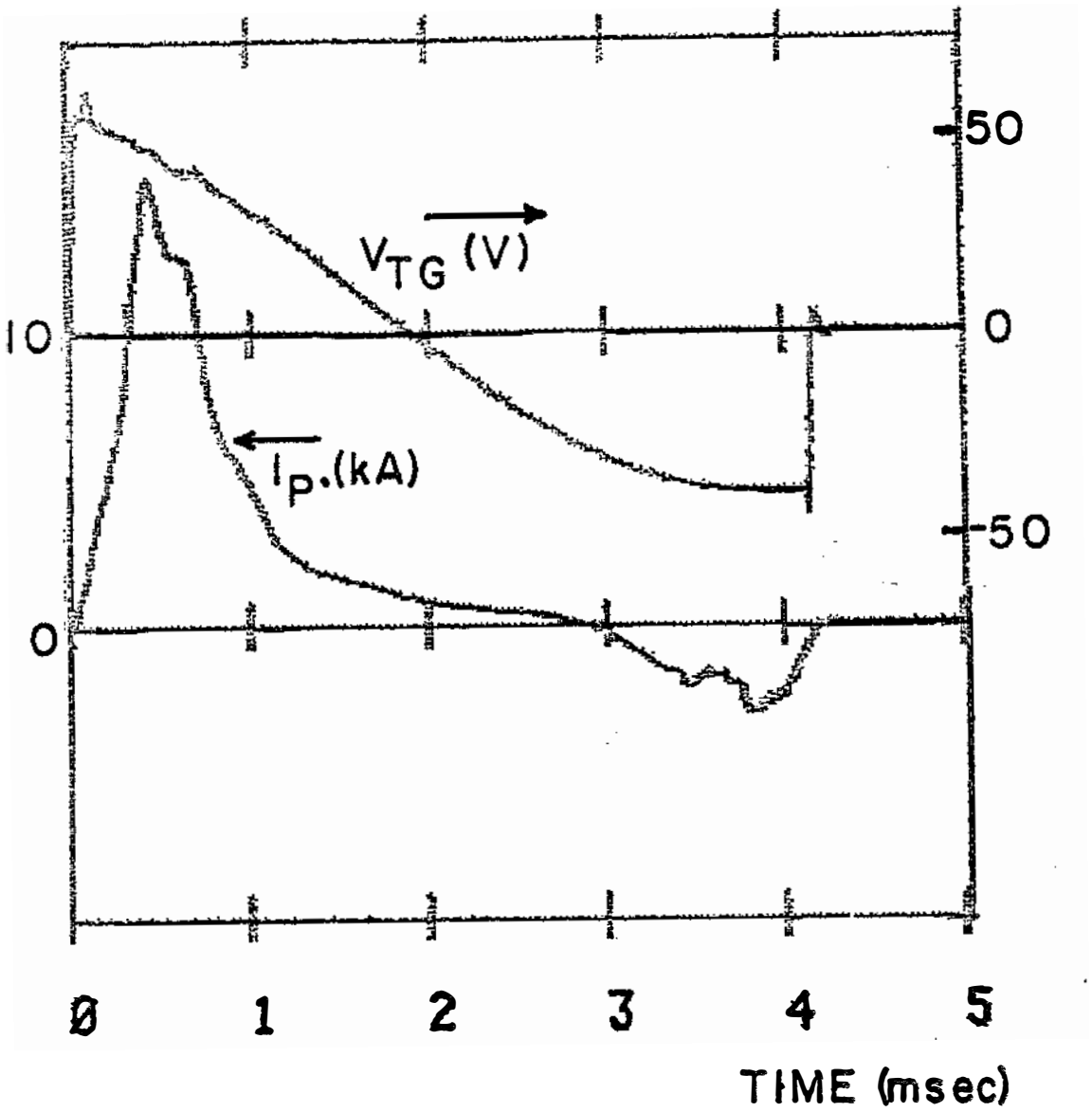


Figure 4. Experimental measurement of plasma current and poloidal loop voltage $V_{TG}$. For this trace the poloidal bank voltage was 2.0 kV, toroidal bank voltage 3.0 kV.

$$\frac{\Delta B_T - \frac{\mu_0}{2\pi R}\Delta I_W}{B_{T(VAC)}} = \frac{I_P}{-I_{W(VAC)}}$$

A typical measurement of $I_R$ vs. R is shown in Fig. 5. Note that the current density is essentially zero between the major axis and R=60 cm, and is roughly constant from R=60 cm to the outer wall.

Fig. 6 and Fig. 7 show the scaling of the peak poloidal current with poloidal loop voltage $V_{TG}$ and with poloidal field (the poloidal loop voltage appears across the toroidal gap, and thus is called $V_{TG}$). The poloidal loop voltage is varied by charging the $B_T$ capacitor bank to different voltages, so that the toroidal magnetic field is proportional to the poloidal loop voltage. This results in several effects as $V_{TG}$ is raised: the poloidal electric field goes up, the angle between the magnetic field and the poloidal electric field increases, and the mirror ratio is reduced. As $B_P$ is raised, the mirror ratio goes up and the field lines become more nearly poloidal. Thus it is not immediately obvious how one should expect the poloidal current to vary with $V_{TG}$ and $B_P$. The poloidal current was

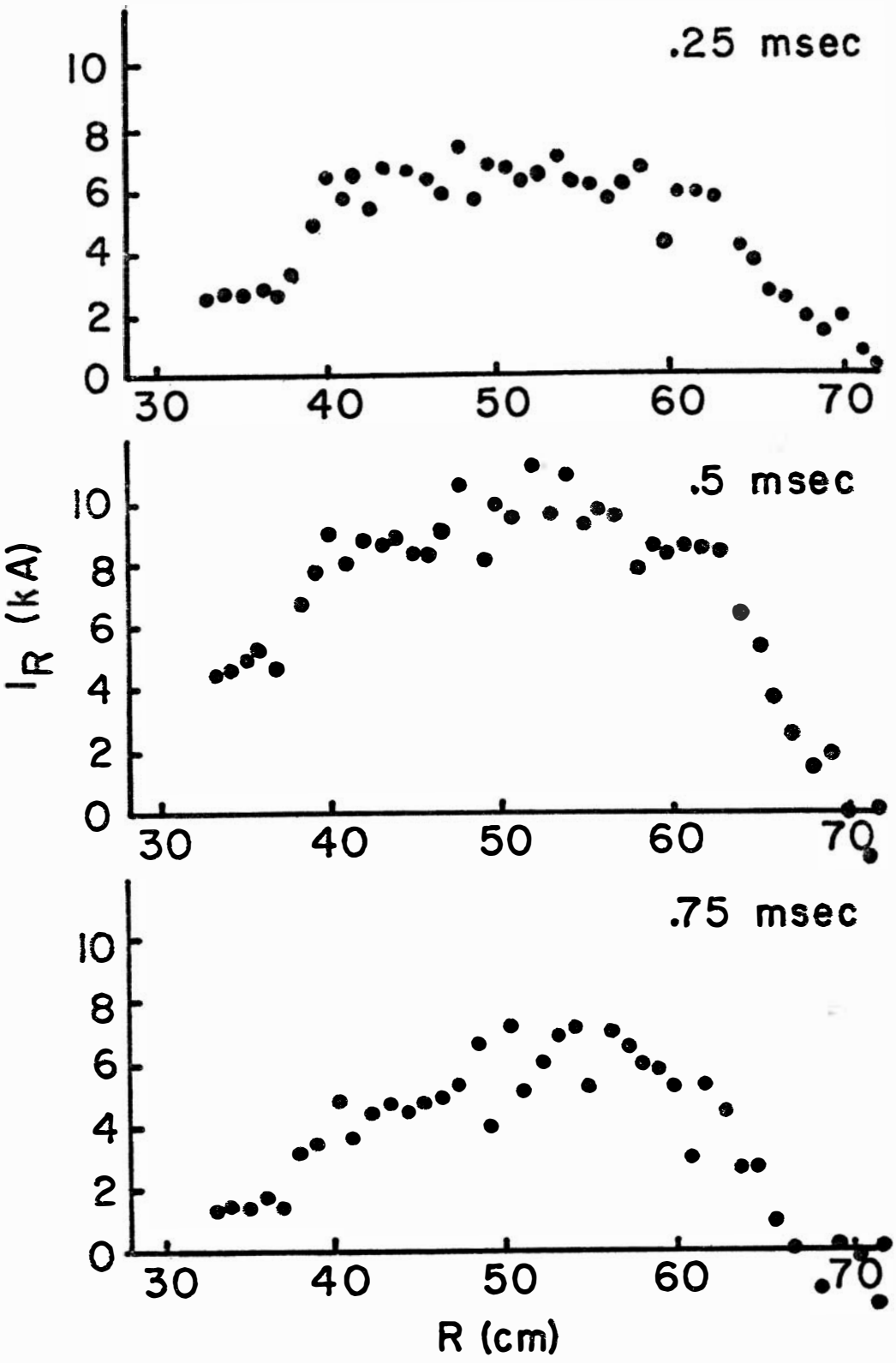


Figure 5. $I_R$ (the total poloidal current between the probe tip and the wall) vs. distance from the major axis. The slope of the curve at a given R is proportional to the total poloidal current in an annulus at that R.

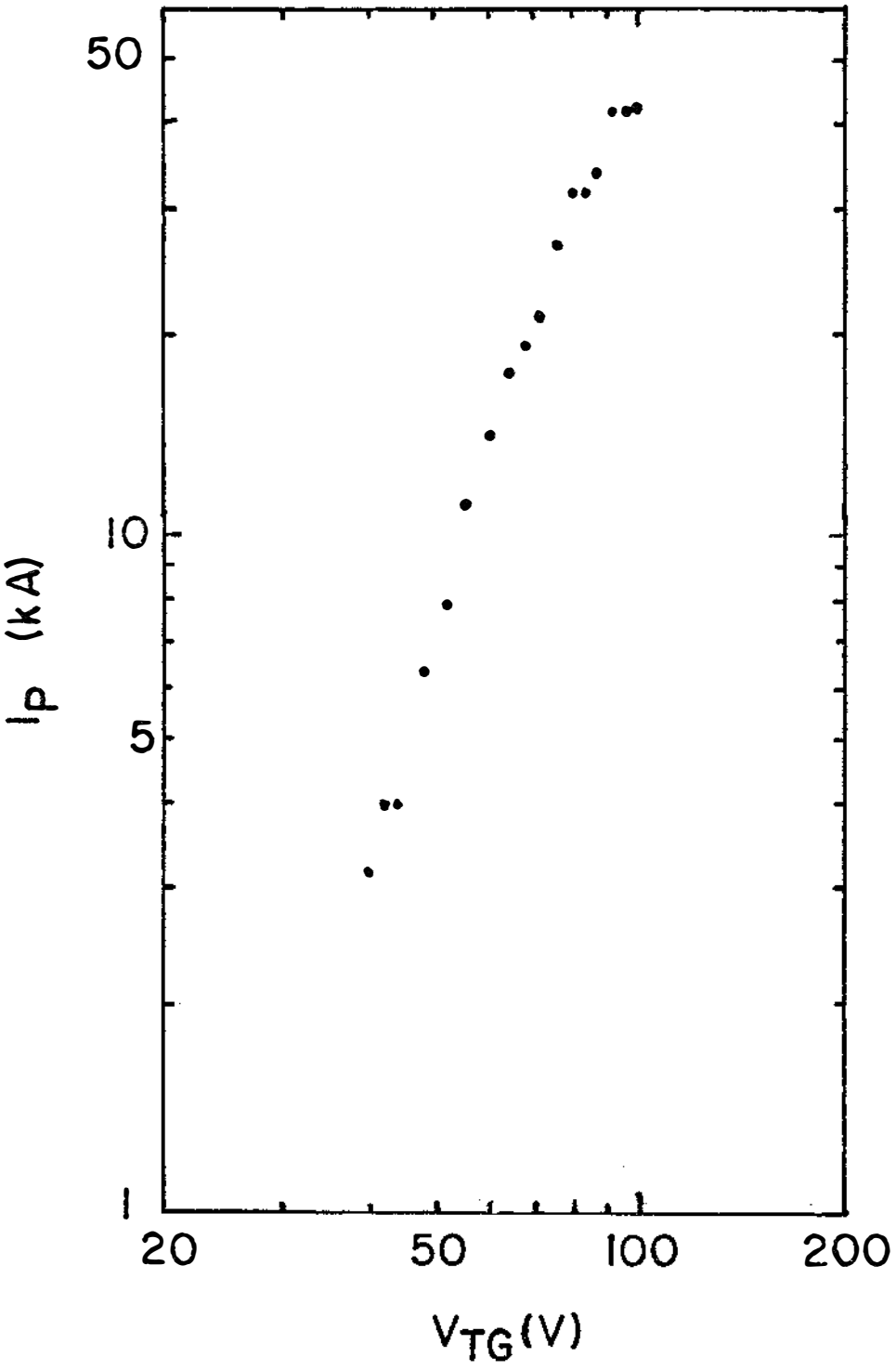


Figure 6. Peak poloidal plasma current vs. poloidal loop voltage $V_{TG}$. The poloidal bank voltage is 2.0 kV.

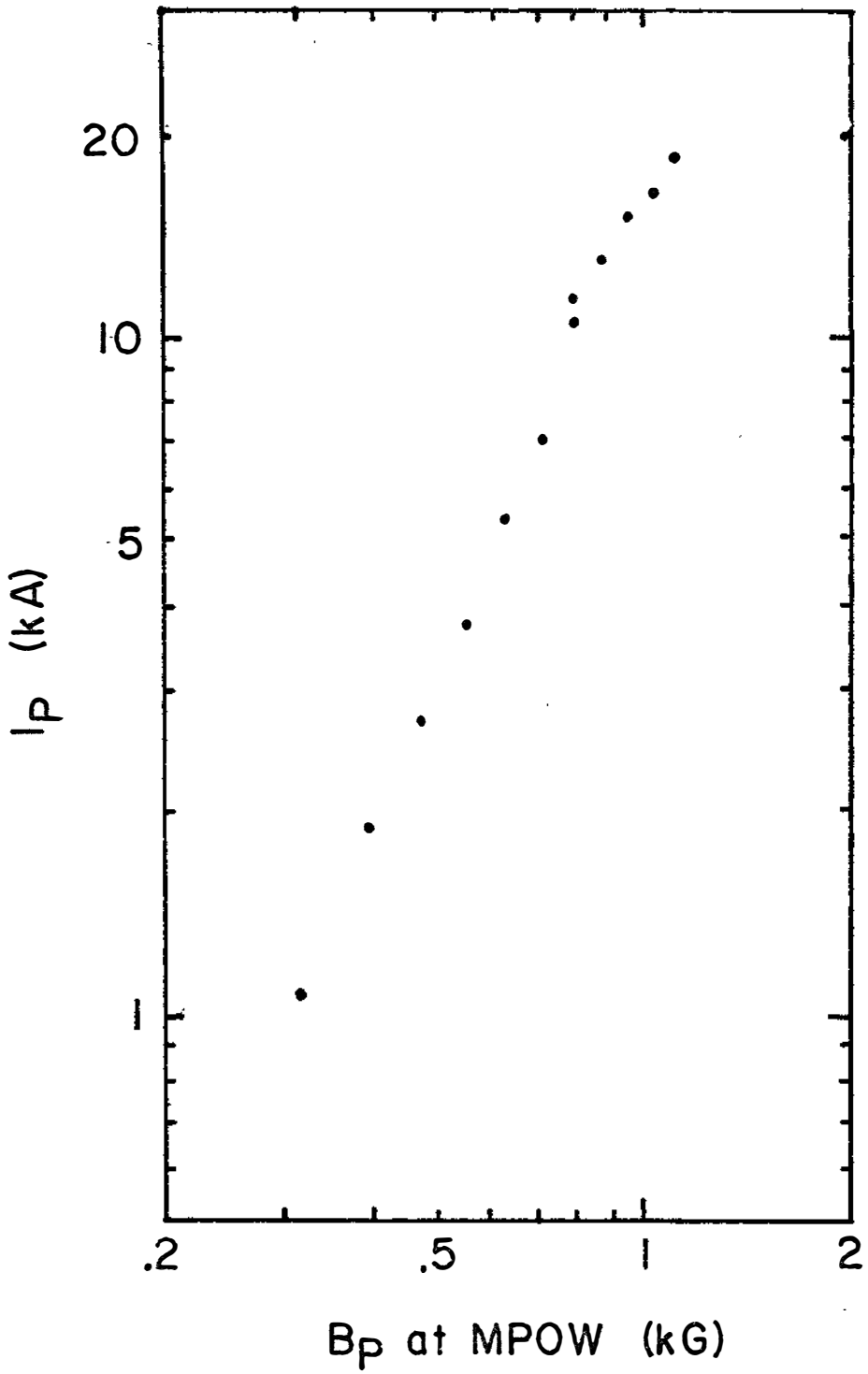


Figure 7. Peak poloidal plasma current vs. poloidal field at midplane outer wall. The toroidal bank voltage is 3.0 kV.

measured over a grid of poloidal loop voltages and poloidal fields and found to fit quite closely to the expression

$$I_P \propto B_P^{1.54} * V_{TG}^{2.55}$$

## DENSITY AND TEMPERATURE MEASUREMENTS

The electron density in the poloidal ohmic heating mode is measured using Langmuir probes and using a microwave interferometer. Generally the interferometer is used as a calibration for the Langmuir probe and the Langmuir probe is used for local measurements and for some scaling studies.

The interferometer is a 40 GHz (unswept) system whose beam passes from the top to the bottom of the vacuum tank. Because the plasma is quite noisy during the heating, it is difficult to count the interferometer fringe shifts while the heating is taking place; to measure the peak density the toroidal field is crowbarred so the plasma decays smoothly, and the fringe shifts are counted during the decay. The density the interferometer measures is a line-average density from the top to the bottom of the machine. For typical poloidal discharges the interferometer measures a density of about $n_e = 4 * 10^{12}$ cm$^{-3}$.

Typical ion saturation current profiles, taken with a floating double probe, are shown in Fig. 8 (midplane scan) and Fig. 9 (bridge scan). Both figures show the evolution of the density profile with time; initially the density is peaked toward the walls, where most of the plasma current is flowing, and gradually shifts inward until it is peaked on the separatrix.

Fig. 8 and 9 also show the percentage fluctuation in the ion saturation current as a function of time and location. The fluctuation is very large (>100%) in the region where the poloidal current flows. After the toroidal field is turned off (at about 4 msec), so there is no poloidal electric field, the fluctuation amplitude is much reduced (Fig. 8f and 9f). Note that while poloidal current is flowing, the fluctuations are very large both when the saturation current profile is peaked toward the walls and when it is peaked toward the separatrix, suggesting that a current-driven, rather than pressure-driven, instability may be responsible for the short confinement times during the ohmic heating.

Several techniques are used to measure the electron temperature; the results of the different techniques are in good agreement. The ratios of intensities of oxygen

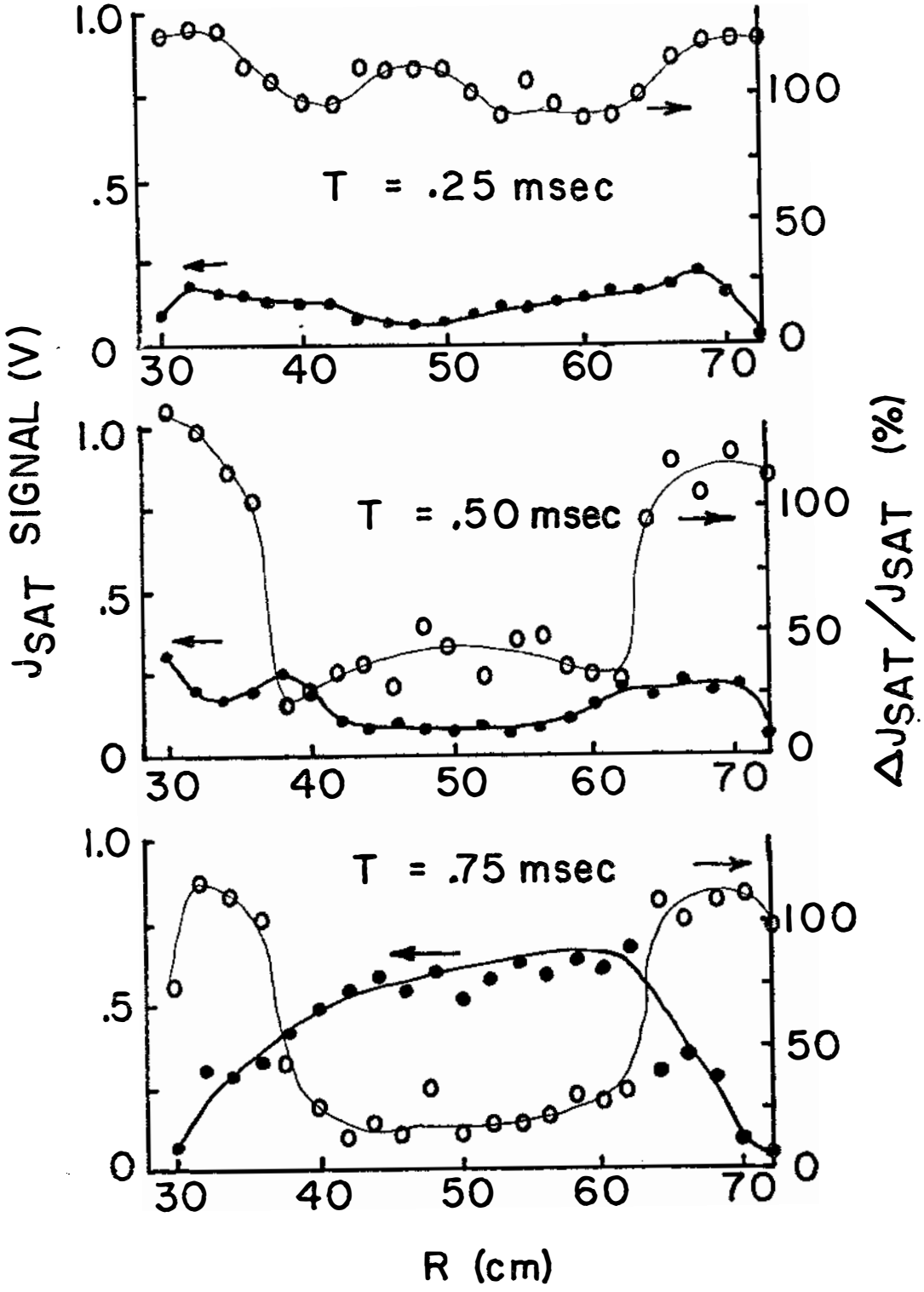


Figure 8 a, b, c. Ion saturation current and percent fluctuation in ion saturation current in midplane for various times after the poloidal electric field is applied. Toroidal bank voltage is 3.0 kV, poloidal bank voltage is 2.0 kV.

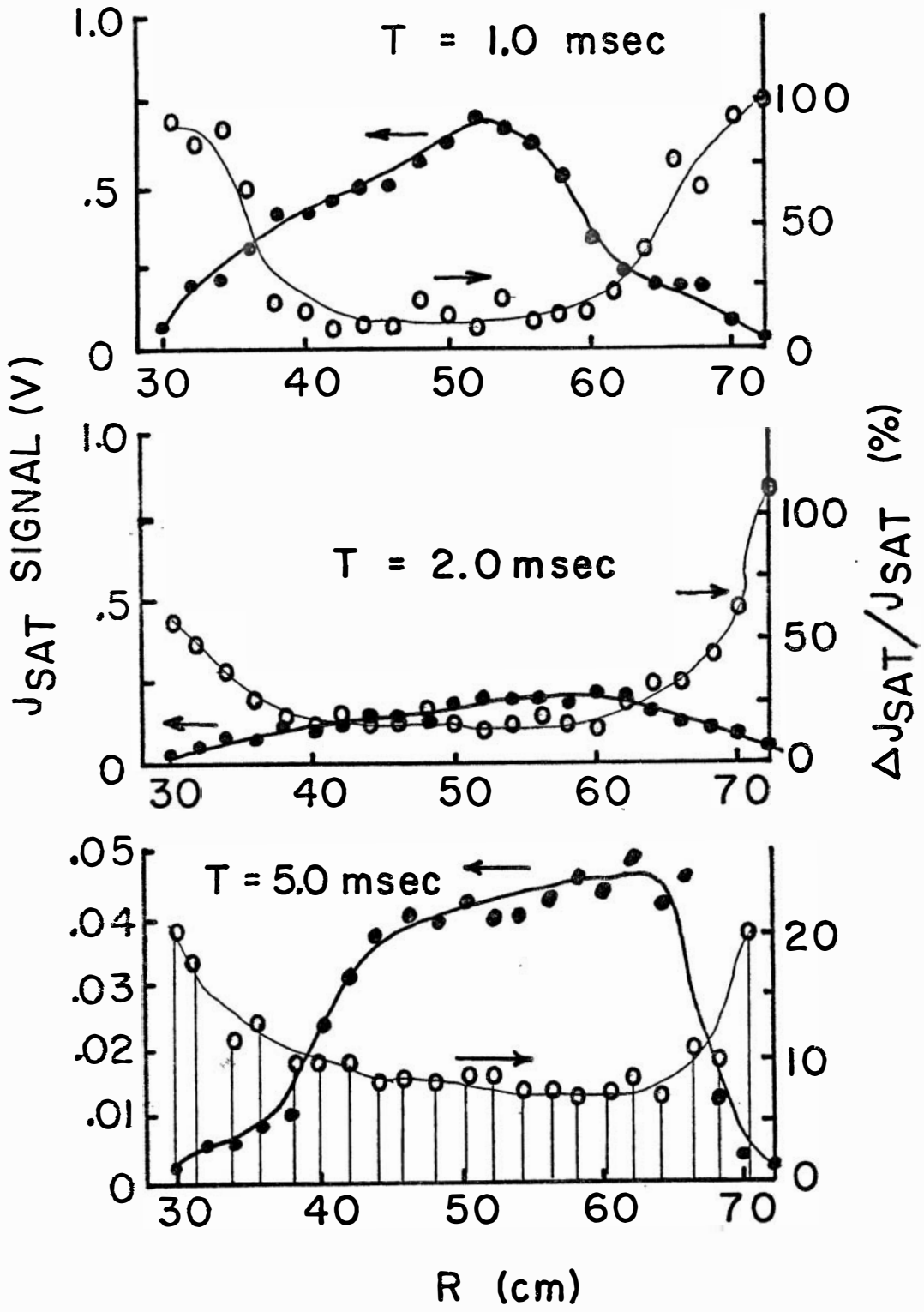


Figure 8 d, e, f. Note the expanded vertical scale in f, also the error bars on the percentage fluctuation in f.

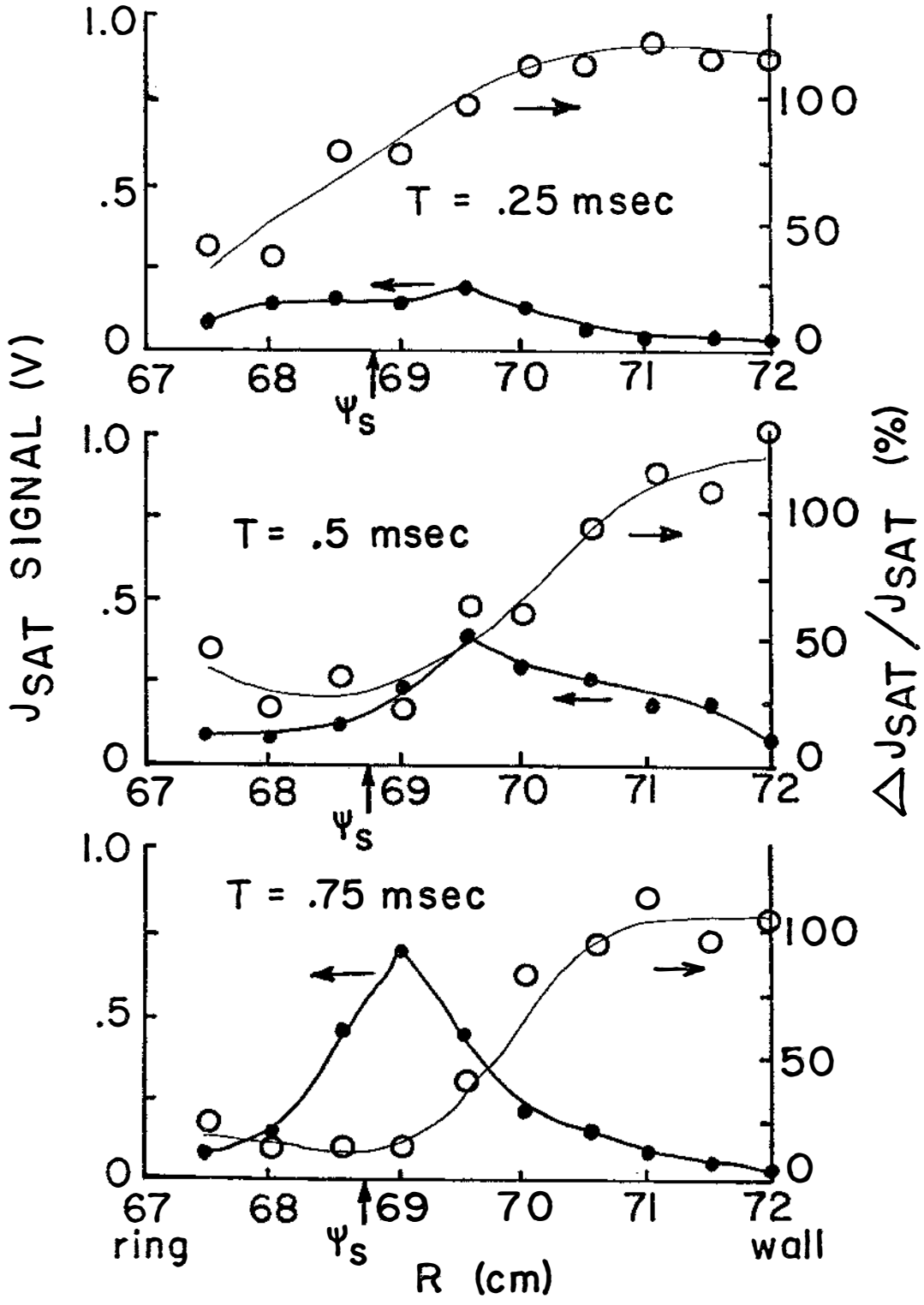


Figure 9 a, b, c. Ion saturation current and percent fluctuation in ion saturation current in bridge region for various times after the poloidal electric field is applied. Toroidal bank voltage is 3.0 kV, poloidal bank voltage is 2.0 kV. $\Psi_s$ indicates the separatrix flux surface.

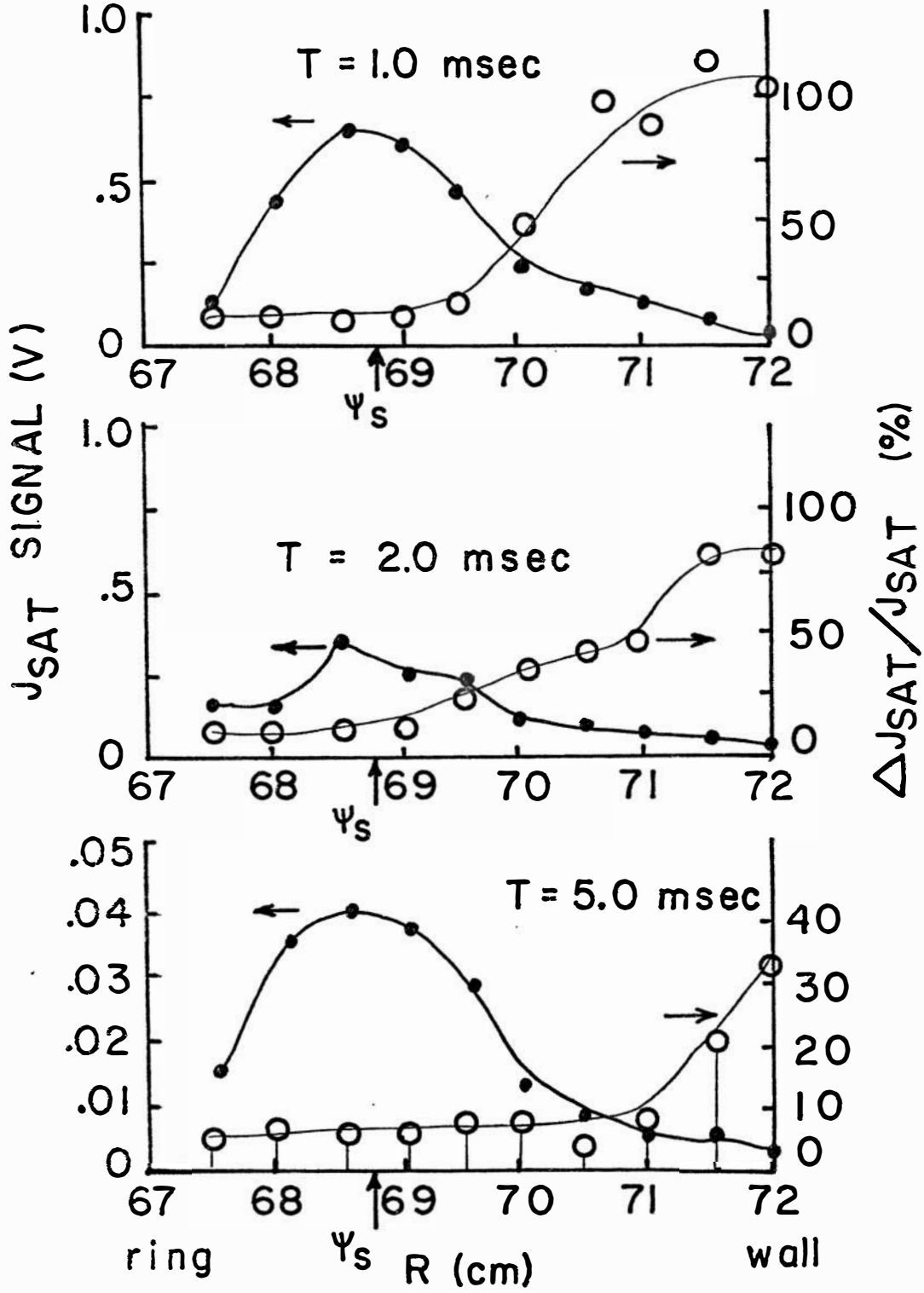


Figure 9 d, e, f. Note the expanded vertical scale in f, also the error bars on the percentage fluctuation in f.

radiation lines give an indication of line-averaged temperature which is quite sensitive to temperature changes. Triple Langmuir probes[2] have also been used to measure $T_e$: a large fixed triple probe in the bridge region at the separatrix is used for scaling measurements and a smaller movable triple Langmuir probe is used for localized $T_e$ measurements. The swept Langmuir probe technique is also used with a small movable probe for localized measurements, using a sweep of several hundred volts with a sweep time of 20 usec.

A typical radial $T_e$ profile obtained with the small triple probe is shown in Figure 10. In general, the electron temperature measurements all indicate that the electron temperature never rises above 15-25 eV and has a fairly flat spatial profile.

## RESISTANCE CALCULATION

The resistance that is measured in these poloidal ohmic heating experiments is

$$R = \frac{V_{11}}{\Delta I_p}$$

Here $\Delta I_p$ is the poloidal plasma current flowing between two

Figure 10. Radial $T_e$ profile taken with small triple probe in midplane. The poloidal bank voltage is 2.0 kV.

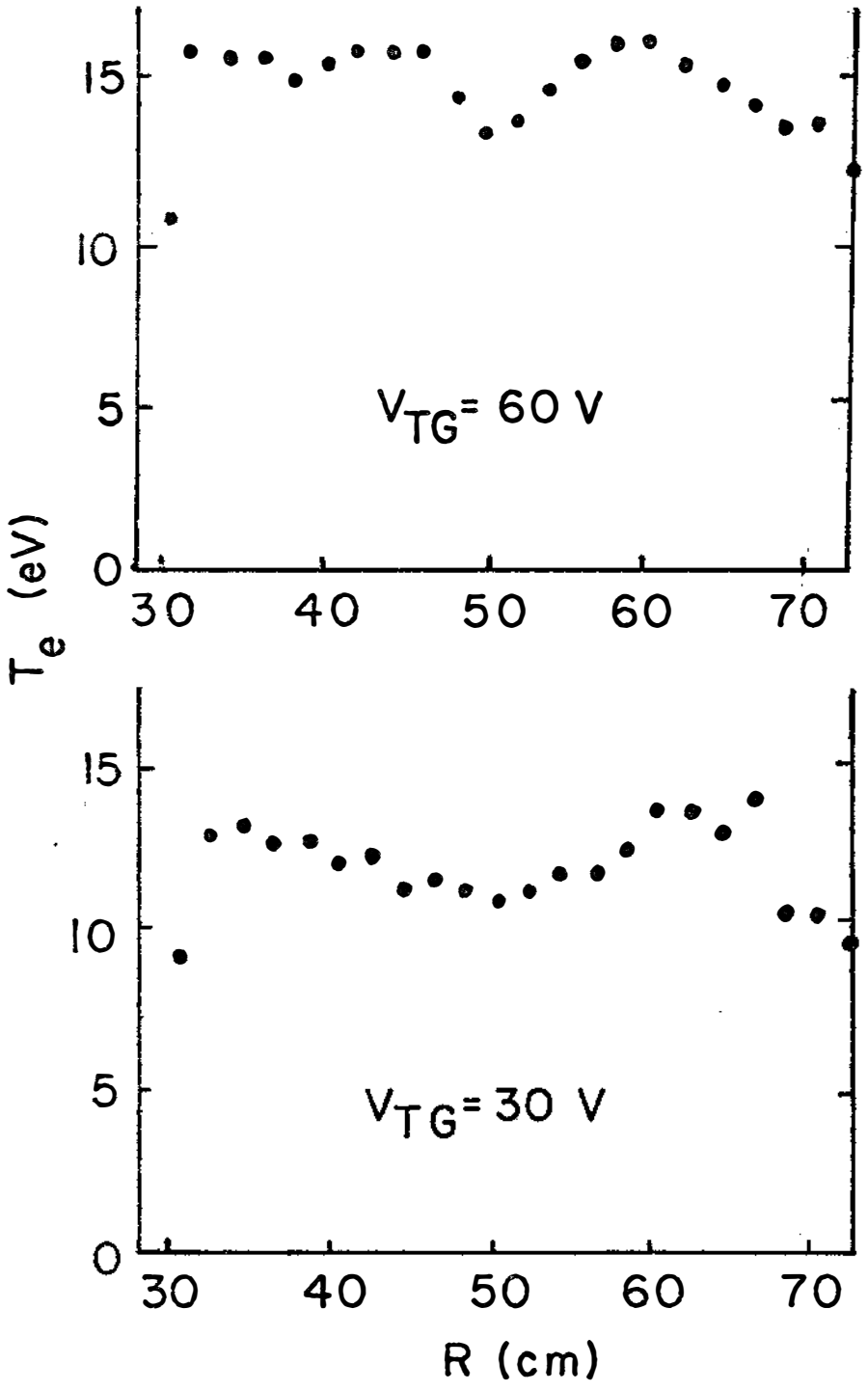

flux surfaces. $V_{ll}$ refers to the voltage between the ends of a flux tube as it goes around once poloidally. This is calculated assuming unperturbed poloidal electric field by a computer program from the equation

$$\vec{E}(\vec{x}) = -\frac{\partial}{\partial t}\vec{A}(\vec{x})$$

$$= -\frac{\partial}{\partial t}\frac{\mu_0}{4\pi}\int\frac{\vec{J}(\vec{x}')}{|\vec{x}-\vec{x}'|}\,d^3x'$$

The program approximates the poloidal surface current flowing on the inside wall of the Tokapole by a series of poloidal filament currents. The hoops are assumed to be perfect conductors; thus each hoop is assumed to carry a poloidal filament current equal and opposite to the wall filament current at each azimuth. The program follows along poloidal field lines, calculating the electric field at uniformly-spaced points along the lines, and summing to get $V_{ll}$. The average electric field along a flux line is shown as a function of flux surface $\Psi$ in Fig. 11 a. Fig. 11 b shows the average electric field along a field line as a function of distance from the major axis for locations in the midplane.

Figure 11. Average electric field once around a poloidal field line vs. flux surface $\Psi$ and vs. distance R from the major axis in the midplane. Toroidal bank voltage is 3.0 kV.

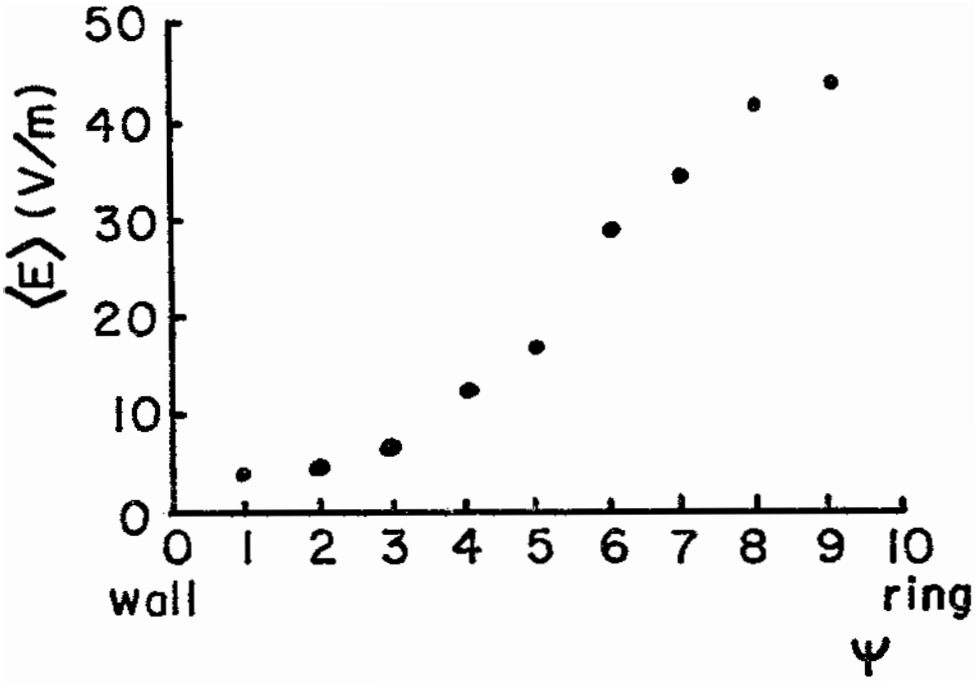


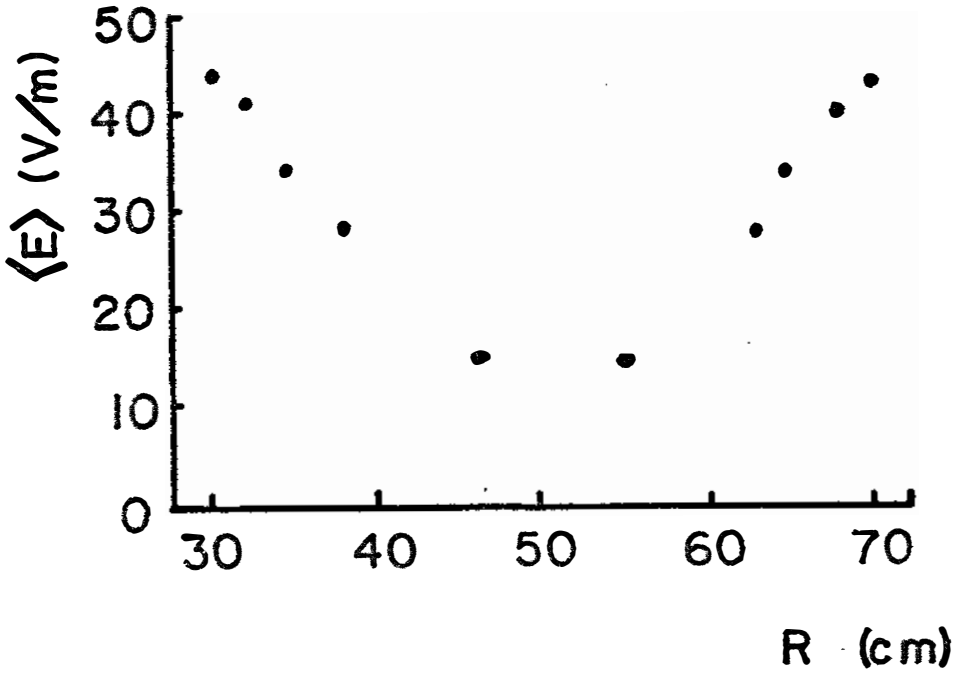

In order to compare this measured resistance to what one would expect assuming Spitzer resistivity, the Spitzer resistivity must be properly averaged over a flux tube as it travels once around the machine poloidally. The calculation must take into account the changing area of the flux tube, as well as its total length, including both toroidal and poloidal fields. The Spitzer resistance for the region between two flux surfaces can be shown[3] to be

$$R_S = \frac{\eta_S \oint \frac{B^2}{B_P} \, dl}{B \, A_{POL} \cos^2 a}$$

Here $\oint \frac{B^2}{B_P} \, dl$ is calculated by summing along field lines for various values of $\alpha$ ($\alpha = B_T/B_P$ at the midplane outer wall). It is shown as a function of $\alpha$ and $\Psi$ in Fig. 12. B is the magnetic field at a given location and $A_{POL}$ is the projection perpendicular to $B_P$ of the total area between the two flux surfaces; a is the angle between B and $B_P$ (Fig. 13). It projects the measured poloidal current and $A_{POL}$ onto the direction perpendicular to the total magnetic field. The denominator is independent of location along the flux tube (since J/B is constant along a flux tube), and is a function only of B, $\Psi$, and $\alpha$.

Figure 12. $\oint \frac{B^2}{B_P} dl$ for various values of $\alpha$ as a function of flux surface $\Psi$. Note that on the separatrix (near $\Psi$=5) the integral goes to infinity, as the separatrix includes the field null ($B_P$ = 0.) The toroidal bank voltage is taken as 5.0 kV; the integral is proportional to poloidal bank voltage.

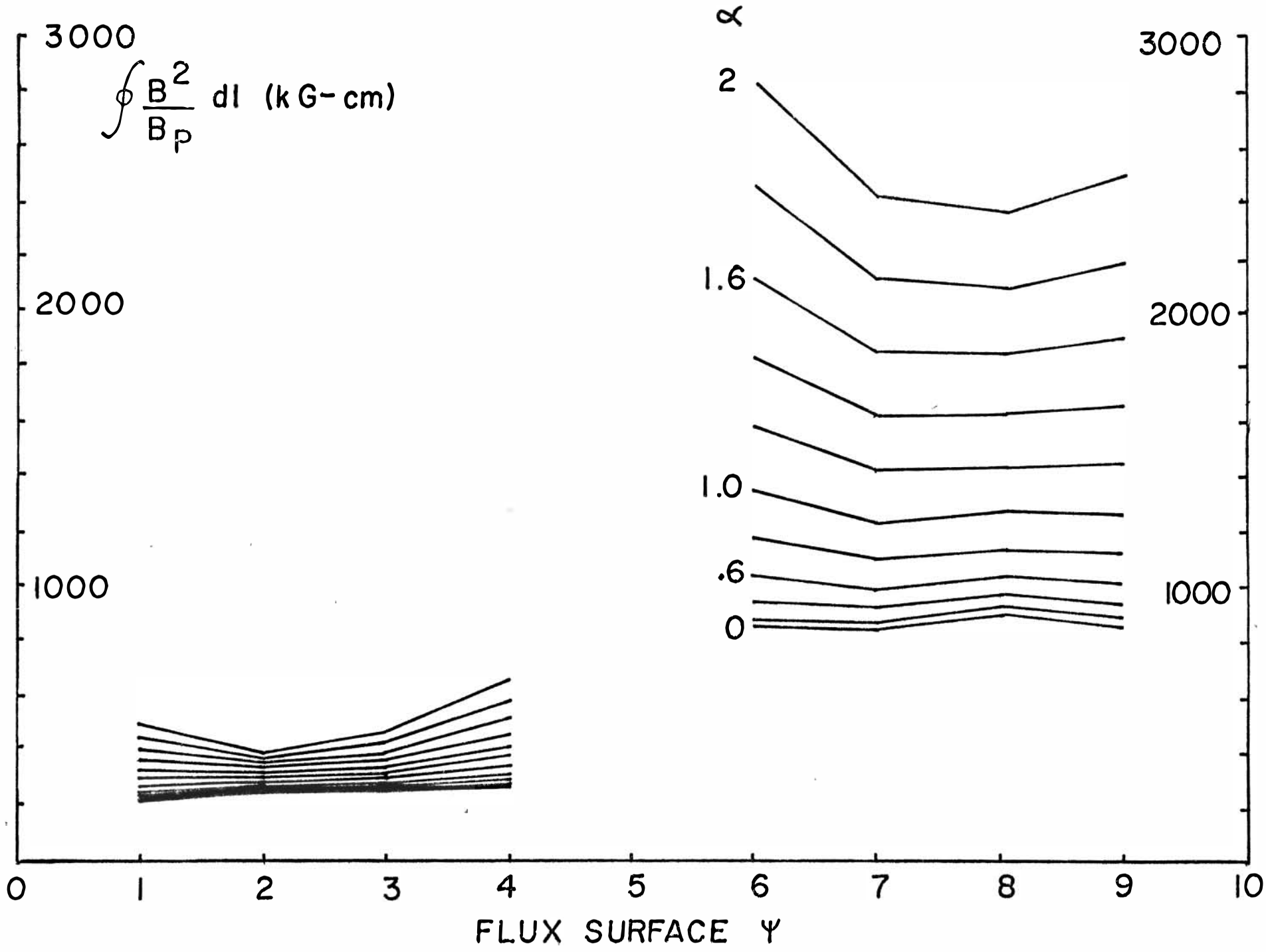
3000
$\oint \frac{B^2}{B_p} dl$ (kG-cm)
2000
1000
α
2
1.6
1.0
.6
0
3000
2000
1000
0
1
2
3
4
5
6
7
8
9
10
FLUX SURFACE Ψ

Figure 13. cos a and $\cos^2 a$ vs. distance R from the major axis on the midplane for various values of $\alpha$. ($\alpha$ is the ratio of $B_T$ to $B_P$ at the midplane outer wall.)

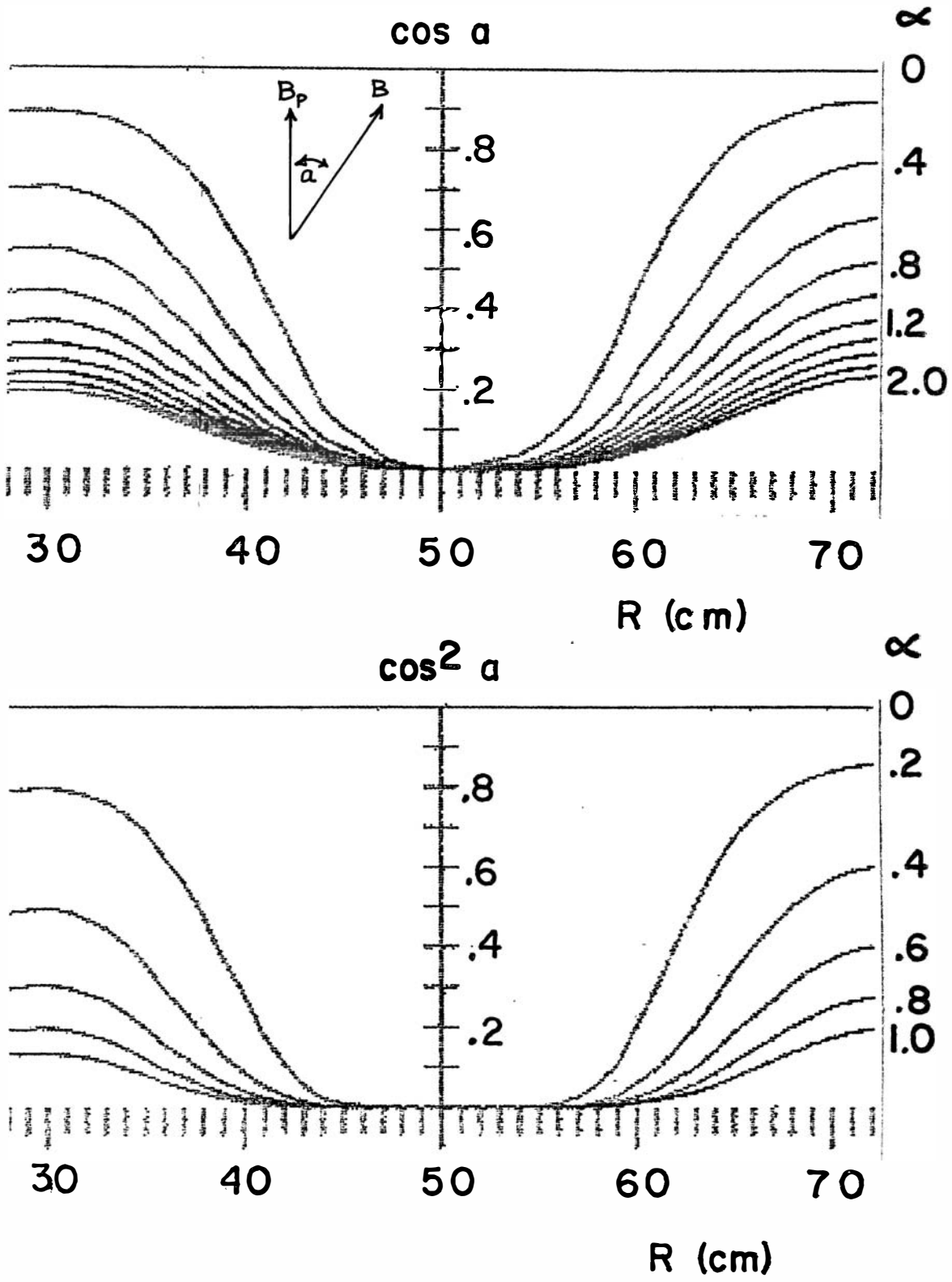

Since almost all of the current flows within 10 cm of the wall (measured at the midplane), the total resistance of this region is usually estimated from the experimental measurements, and compared to the corresponding Spitzer resistance as calculated above. The values obtained experimentally typically range from slightly greater than the Spitzer resistance to about 15 times that value.

Since the mirror ratio on the flux surfaces where the current flows ranges, for typical values of $\alpha$, from about 4 to about 8, one would expect resistances ranging from about 20 to 75 times the Spitzer resistance if the effect of the octupole mirrors dominated collisional effects.[4] However, for our plasma parameters, the electron-ion collision frequency $\nu_{ei}$ and the bounce frequency $\nu_b$ between the magnetic mirrors are comparable, so that the resistance we measure should be somewhere between the Spitzer value and a collisionless mirror-dominated resistance. Thus the measured resistances are not surprising. The ratio of measured resistance to Spitzer resistance rises as $\nu_{ei}/\nu_b$ gets smaller, as would be expected.

## CONFINEMENT TIME AND SCALING

The poloidal current, electron density, and electron temperature (the latter two via a large fixed triple Langmuir probe in the bridge region) were monitored for a wide range of poloidal loop voltages and poloidal fields; The results are shown in Fig. 14, 15, and 16. Note that the density and plasma current increase with $V_{TG}$ and $B_P$ up to the highest values examined, but the electron temperature seems to saturate around 20 eV. This saturation is confirmed by optical measurement.

From the observed current, density and temperature, one can estimate an energy confinement time

$$\tau_E = \frac{nkT_e}{\int V_{ll}\, dI_P}$$

which typically comes out to only a few microseconds. This is to be compared to a confinement time of about a millisecond after the ohmic heating is turned off. Furthermore, the saturation of $T_e$ with increasing plasma current means that the energy confinement time is decreasing with increasing heating power input.

Figure 14. Electron density at time of peak plasma current as a function of poloidal field at midplane outer wall and poloidal loop voltage $V_{TG}$.

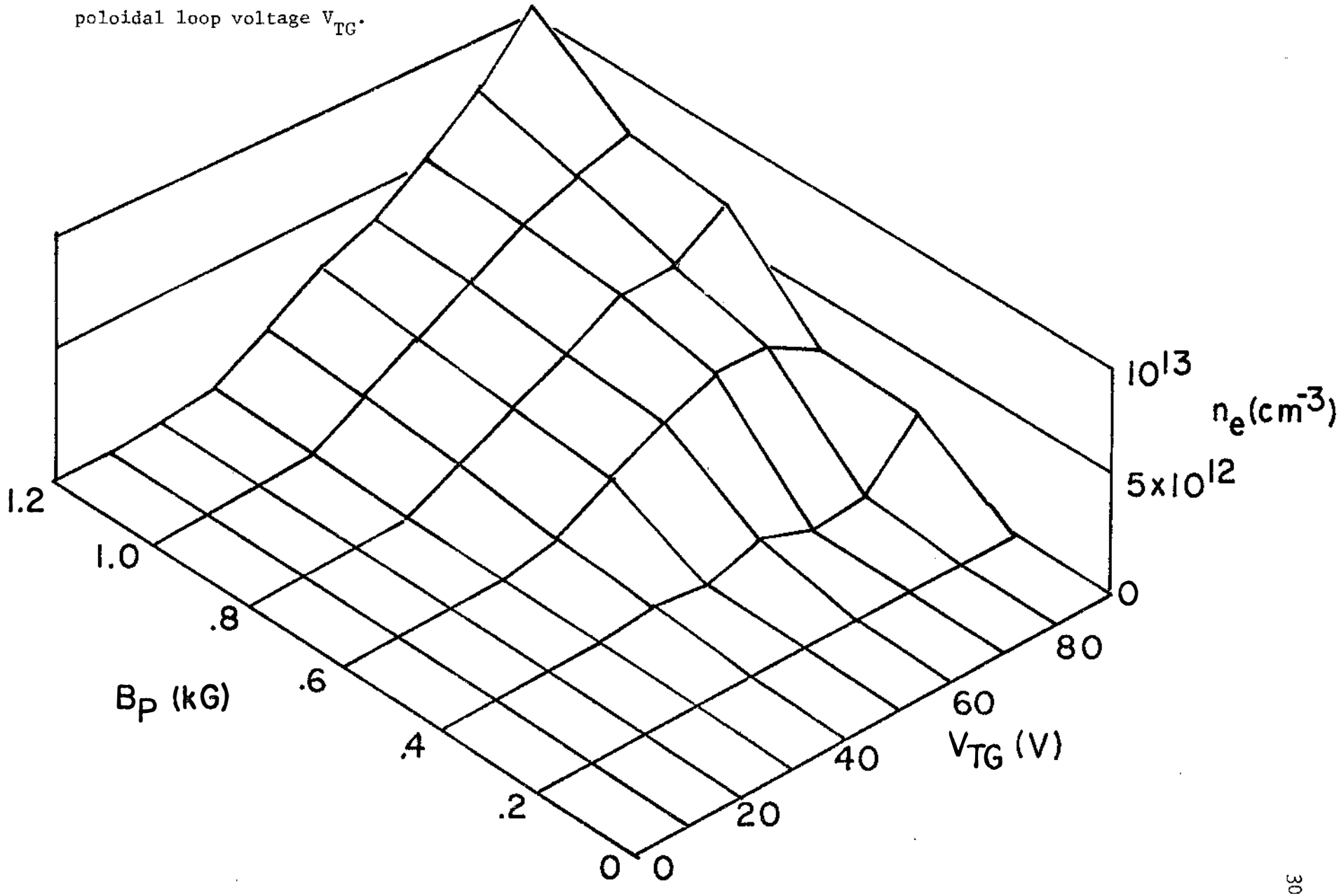

Figure 15. Peak poloidal plasma current as a function of poloidal field at midplane outer wall and poloidal loop voltage $V_{TG}$.

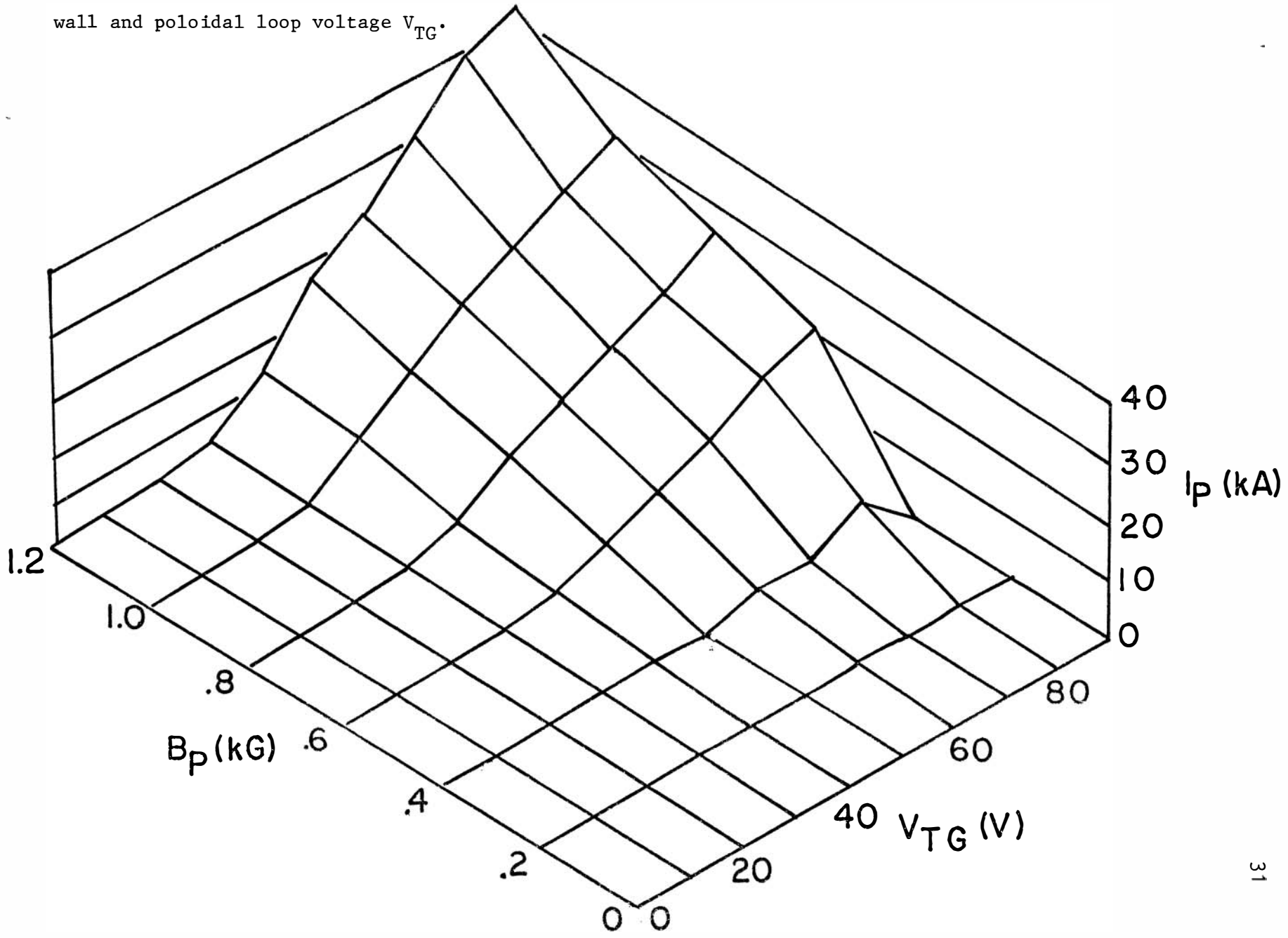

Figure 16. Electron temperature at time of peak plasma current as a function of poloidal field at midplane outer wall and poloidal loop voltage $V_{TG}$.

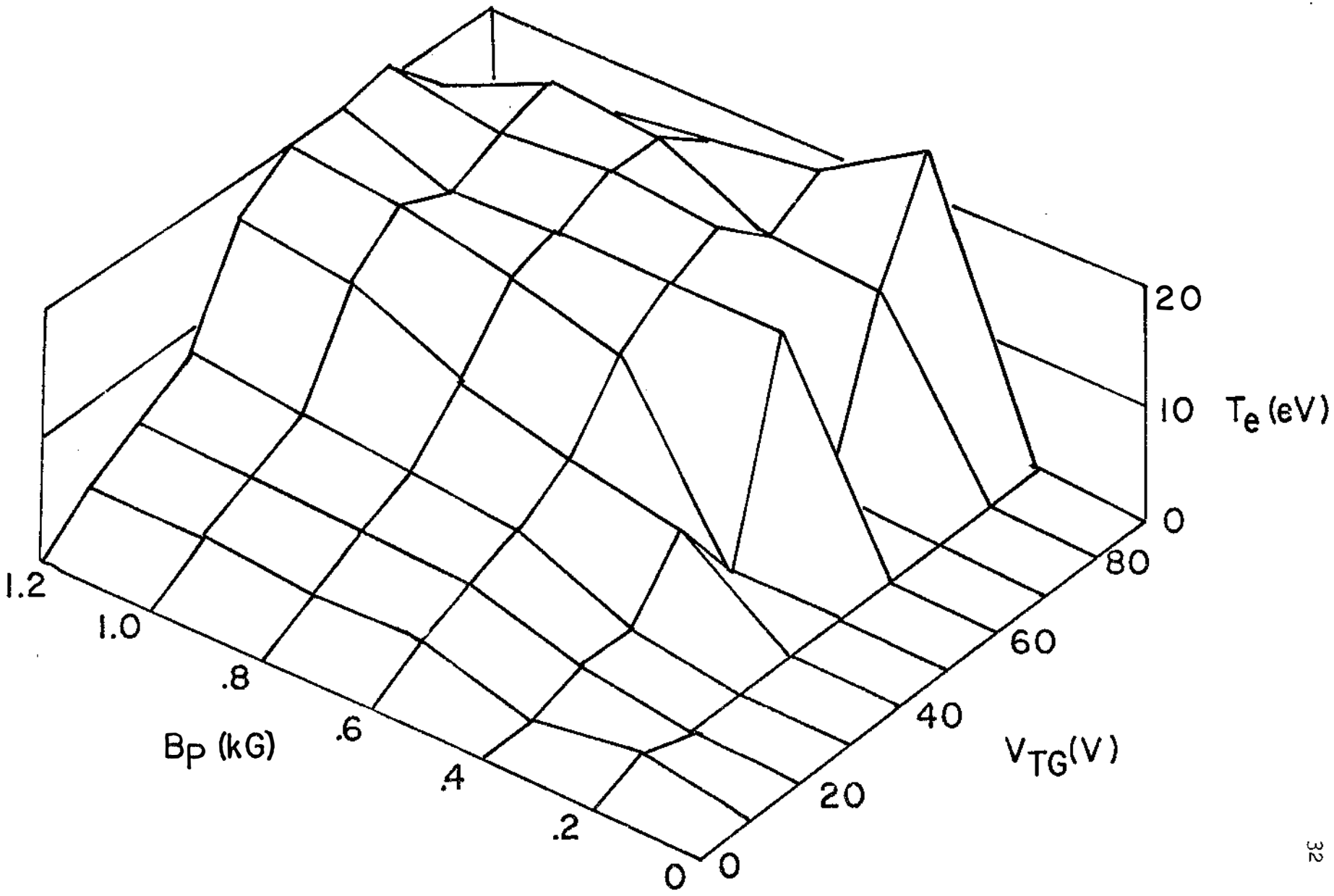

We are currently trying to discover the mechanism for the electron temperature saturation. It is unknown whether the energy confinement time is limited by particle losses or by some other mechanism. The cleanliness of the walls seems to play an important role in determining the energy confinement time; this is not surprising since the hottest densest part of the plasma is near the wall. An improved discharge cleaning scheme which is currently being implemented may lead to an improvement in plasma parameters.

REFERENCES

1. Don Holly and Tom Lovell, "Op amp reduces transformer droop", EDN, October 5, 1979

2. S-L Chen and T. Sekiguchi, J. Appl. Phys. 36, 2363 (1965); J. C. Sprott, PLP 109 (1967)

3. This is a slightly modified form of an expression derived in D. A. Brouchous and J. F. Etzweiler, submitted to Phys. Fluids

4. D. A. Brouchous and J. F. Etzweiler, op. cit.